Spectral evolution of GRB 060904A observed with *Swift* and *Suzaku*

Daisuke Yonetoku,[1] Sachiko Tanabe,[1] Toshio Murakami,[1] Yuka Aoyama,[1] Takashi Kidamura,[1] Hironobu Kodaira,[1] Shinya Okuno,[1] Satoru Yoshinari,[1] Keiichi Abe,[2] Kaori Onda,[2] Makoto S. Tashiro,[2] Yuji Urata,[2] N. Ishikawa,[3] Yujin E. Nakagawa,[3] Satoshi Sugita,[3] Kazutaka Yamaoka,[3] Atsumasa Yoshida,[3] Takuto Ishimura,[4] Nobuyuki Kawai,[4] Takashi Shimokawabe,[4] Kenzo Kinugasa,[5] Takayoshi. Kohmura,[6] Satoshi Eguchi,[7] Kaori Kubota,[7] Yoshihiro Ueda,[7] Kazuhiro Nakazawa,[8] Tadayuki Takahashi,[8] Shouta Maeno,[9] Eri Sonoda,[9] Makoto Yamauchi,[9] Makoto Kuwahara,[10] Motoko Suzuki,[10] Toru Tamagawa,[10] Ken'ichi Torii,[11] George Ricker,[12] Lorella Angelini,[13] Scott Barthelmy,[13] L. J. Kaluzienski,[13] Richard L. Kelley,[13] James N. Reeves,[13] Neil Gehrels,[13] and John Nousek,[14]

[1]*Department of Physics, Kanazawa University, Kakuma, Kanazawa, Ishikawa 920-1192, Japan*
yonetoku@astro.s.kanazawa-u.ac.jp (DY)

[2]*Saitama University, Sakura, Saitama, 338-8570, Japan*

[3]*Aoyama Gakuin University, Sagamihara, Kanagawa, 229-8558, Japan*

[4]*Tokyo Institute of Technology, Ohokayama, Meguro, Tokyo, 152-8551, Japan*

[5]*Gunma Astronomical Observatory, Takayama, Gunma, 377-0702, Japan*

[6]*Kogakuin University, Hachioji, Tokyo, 192-0015, Japan*

[7]*Kyoto Univsersity, Sakyo-ku, Kyoto, 606-8502, Japan*

[8]*JAXA/Institute of Space and Astronautical Science, Sagamihara, Kanagawa, 229-8510, Japan*

[9]*University of Miyazaki, Gakuen-kibanadai, Miyazaki, 889-2192, Japan*

[10]*RIKEN, Wako, Saitama, 351-0198, Japan*

[11]*Osaka Univsersity, Toyonaka, Osaka, 560-0043, Japan*

[12]*Massachusetts Institute of Technology, CSR, Cambridge, MA 02139, USA*

[13]*NASA/Goddard Space Flight Center, Greenbelt, MD 20771, USA*

[14]*Pennsylvania State University, University Park, PA 16802, USA*

(Received 2000 December 31; accepted 2001 January 1)

Abstract

We observed an X-ray afterglow of GRB 060904A with the *Swift* and *Suzaku* satellites. We found a rapid spectral softening in the prompt tail observed by *Swift*. Adopting the absorbed power-law model to the observed spectra, the photon indices rapidly change from $\Gamma = 1.2 \pm 0.1$ to $\Gamma = 5.3^{+0.7}_{-0.6}$. It is quite difficult to explain this ultra soft spectrum by the simple electron acceleration and the synchrotron radiation.

Then we try to advanced spectral fitting with the broken power-law with exponential cutoff (BPEC) model, and the power-law with blackbody as seen in GRB 060218. The observed spectra can be explained by the both models. After the transition to the shallow decay phase, the spectral photon indices become steady as the typical value of $\Gamma \sim 2$, and this value keeps flat toward the end of *Suzaku* observation. Through these observation, we confirmed that no significant spectral evolution was found during the shallow–classical–jet break phases.

Key words: gamma rays: burst — radiation mechanisms: non-thermal — relativistic jet — X-rays: individual (GRB 060904A) — X-rays: stars acceleration of particles

1. Introduction

Recent *Swift* observations reveal various behavior about early X-ray afterglows of Gamma-ray bursts (GRBs). Nousek et al. 2006 summarized that their X-ray lightcurves can be classified in three basical phases; the very steep decay, the shallow decay and the classical decay, respectively. The *Swift*/XRT observed additional strong X-ray flares during the very steep decay and the shallow decay phases in a lot of GRBs. However, we can mention that all of these variations are not observed in all GRBs. The jet break as seen in many optical afterglow has been also observed in X-ray lightcurve, but Sato et al. 2006 reported that the X-ray afterglow of GRB 050416A lacks its own jet break over ~ 100 day since the burst trigger time. This fact means that the jet opening half angle is $\theta \geq 23$ degree which is much wider than ever known. On the other hand, for GRB 060105, Tashiro et al. 2007 found a very early jet break before 0.04 day since the GRB trigger time with the *Swift* and *Suzaku* combined observation. Therefore we can say that these temporal charactaristics are case by case. We need much more information about the early X-ray afterglow to comprehend these complex charactaristics.

Several authors reported significant spectral softening during the early X-ray afterglows. Especially, Zhang, Liang & Zhang 2006 performed simaltanious spectral analyses for the brightest 17 cases of X-ray afterglows observed by the *Swift*/XRT. In their report, 10 of 17 samples show strong spectral evolution while the others have no evolution. These spectral evolutions are generally discussed with the curvature effect of emitting materials. Then the spectral and the temporal indices have to show co-evolution when we consider the simplest curvature effect. However the observed spectral evolutions do not match with the property of temporal decline, so Zhang, Liang & Zhang 2006 introduced another hidden component as the central engine afterglow which may be related to the continuous activity of GRB central engines. These characteristics should be investigated in detail because the cases with spectral softening may be a main population of long GRBs.

Using the BATSE data, Ryde 2005 investigated the possibility of existence of the thermal

emisson in the prompt GRB spectra. He described the prompt emission spectra with the thermal (blackbody) spectrum combined with the non-thermal (power-law) one. Butler 2006 also explained the GRB 060218 showing anomalous soft X-ray spectra as the thermal + non-thermal model. He suggested that the X-ray afterglow of dominated by thermal emission with the effective temperature of $kT \sim 0.3$ keV compared with the non-thermal emission. Even if, including the thermal emission, the spectral evolution of the power-law component still remains, and the photon indices change from $\Gamma = 1.5$ to $\Gamma = 3.4$. Therefore, additional inoformations are required.

In this paper, we show the observation results of GRB 060904A with the *Swift* and *Suzaku* satellites. This event show one of the strongest spectral softening ever observed, and the spectral phoson index achieve $\Gamma = 5.3^{+0.7}_{-0.6}$. In the next section, we summarized the X-ray observations for this event. In the third section, we performed the temporal and the spectral analyses. We try to adopt three possible models (the single power-law, broken power-law with exponential cutoff, the blackbody with power-law) to the observed spectra, and summarize the fitting results. We succeeded to resolve the prompt tail and/or X-ray flare from the X-ray afterglow. In the final session, we discuss about the possible origin to interpret the ultra soft spectra.

2. Observations

GRB 060904A was detected by the BAT instrument aboard the *Swift* satellite at 2006/09/06 01:03:21 (UT), and localized at R.A. $= 15^h50^m58^s$, Dec. $= +44^d57'57"$ (J2000) with the uncertainty of 3 arcminutes. The BAT lightcurve shows several little peaks and then an intense flare composed by multi spikes at $t - t_0 \sim 55$ sec. Here t_0 is the GRB trigger time. The burst duration time measured at the BAT energy range was about $T_{90} \sim 85$ sec.

The XRT automatically started the follow-up observation from $t - t_0 = 66$ sec with the windowed timing mode. A bright X-ray afterglow was found at R.A. $= 15^h50^m54^s.9$, Dec. $= +44^d59'07.8"$ (J2000) with an estimated uncertainty of 5.4 arcseconds. The initial flux measured by the first 0.1 sec image was 2.7×10^{-8} erg cm^{-2}s^{-1} (0.2–10 keV band). Unfortunately, *Swift* entered the South Atlantic Anomaly at 01:43:52 (UT), and the XRT observation was interrupted by the next GRB 060904B triggered at 02:31:03 (UT). Therefore the XRT data lasted only about 2000 seconds since the burst trigger time.

The X-ray intensity reported by the *Swift*/XRT team was quite intense and the GRB trigger time satisfied with the time of opportunity (ToO) observation by the Japanese X-ray satellite *Suzaku*. The *Suzaku* began the followup observation with the HXD nominal pointing mode from 10:29:46 (UT) to 2006/09/05 05:03:46 (UT) with the net exposure time of 30.4 ksec. We confirmed the X-ray afterglow found by the *Swift*/XRT within the XIS field of view. Therefore *Suzaku* complementary covered the late time behaviour of X-ray afterglow which could not be observed by *Swift*.

No optical counterpart was reported, so this burst was categorized as optically dark GRB. The *Subaru* telescope observed the field of GRB 060904A with MOIRCS near-infrared camera after ~ 5 hours since the burst trigger. An extended object was found within the XRT error circle, but it is still in debate whether the object is the host galaxy of GRB 060904A or not. We have no direct information about the redshift, so we use the possible redshift of $pz = 1.84 \pm 0.85$ calculated with the luminosity indicators e.g. Amati, Yonetoku when we discuss the physical quantities measured at the GRB's rest frame.

3. Data Reduction

The *Swift*/BAT and XRT were analyzed by the standard analysis tools within heasoft 6.1.2 packages.

For the windowed timing mode data of XRT, using xselect software, we extracted both X-ray afterglow and background spectra within rectangle regions of 40 pixels in width with a height large enough to include all the photons. We used the energy response matrix file (RMF) released by the XRT team, and the aucillary response file (ARF) are generated for each spectral file with the "xrtmkarf" command including the latest calibration database.

We divided the *Swift*/XRT data into 22 time intervals as shown in figure 1. Since the

X-ray count rate is quite high just after the start of XRT's pointing observation, we removed the brightest 4 pixels from the central field of extracted source region to deal with the pile-up effect until $t - t_0 \leq 86.55$ sec. As shown in the X-ray lightcurve, we can recognize 2 remarkable X-ray flares around 300 sec and 700 sec. We divided the XRT data to trace the arising and decaying behaviors for these two X-ray flares. Although the first steep decay (prompt tail) has several fluctuations in X-ray intensities, we will not discuss their temporal behaviour in detail because their emission powers are dominated by the base line of main prompt tail.

We used observation data with the procesing version of rev1.2 for both the *Suzaku*/XIS and HXD data, and we also used heasoft 6.1.2 packages when we performed the data reduction. For the XIS data, we took the source region as the circle of 4.34 arcmin in radius, and the background region as the same radius from the opposite side against the optical axis of the X-ray telescope. Since we found a dim source in the background region, we removed it with smaller circle of about 2 arcmin in radius. We generated an RMF and an ARF files with "xisrmfgen" and "xissimarfgen" tools including the latest calibration data base, respectively. For the *Suzaku*/XIS data, we divided it into 5 time intervals and performed spectral analyses.

The 16 HXD-PINs in the well unit number of W0 are operated by bias voltage of 400 V since 2006 May 24, to suppress the rapid increase of noise events possibly caused by the in-orbit radiation damage. The others are operated by nominal bias of 500 V. Therefore we excluded the data obtained by 16 PINs in the W0 unit to avoid large uncertainty of inorbit calibrations. We used the non X-ray background (NXB) event data produced by the HXD team, and performed standard data reduction for 48 PINs in W1, 2, and 3 units. Then the cosmic X-ray backbround (CXB) is not included in the NXB event data, so we modeled the functional form of the CXB based on the past observations. The recomended RMF for the point source observed by the HXD nominal mode, was adopted when we performed the spectral analyses.

The spectral fitting was performed using the XSPEC 12 packages for both *Swift* and *Suzaku* data. Hereafter the quoted errors are at the 90 % confidence level.

4. Spectral and Temporal Analyses

4.1. Single Power-law Fitting

We investigated the spectral evolution for these 27 data set with a simple absorbed power-law model. Here, we deal the galactic absorption $N_{\rm H}^{gal} = 1.41 \times 10^{20}$ cm^{-2} as the fixed parameters (Dickey & Lockman 1990), and the extra galactic (e.g. GRB host) absorption $N_{\rm H}^{ext}$ as the free parameter with the redshift of $pz = 1.84$. In figure 2, we show the temporal history of the X-ray energy flux in 2–10 keV band, the photon index (Γ), and the extragalactic absorption ($N_{\rm H}^{ext}$), respectively. The temporal index of initial steep decay can be explained by power-law as $(t - t_0)^{-6.5 \pm 0.3}$ for the time interval of No. 1–12. We can recognize the flux level of shallow decay phase is almost constant. For the late time suzaku observation, we can described

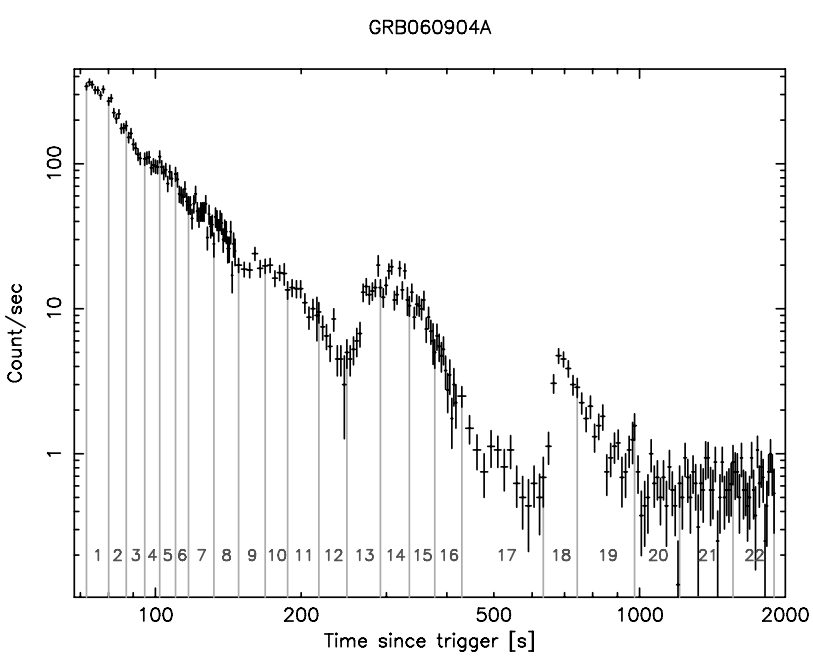

Fig. 1. The lightcurve of the early X-ray afterglow of GRB 060904A observed with *Swift*/XRT. We performed time resolved spectral analyses for 22 divisions as shown in this figure.

the temporal decay as $(t-t_0)^{-2.3\pm0.3}$ which is consistent with the steeper decay phase after the jet break. The photon indices show the remarkable and continuous softening during the steep decay phase from $\Gamma = 1.2 \pm 0.1$ to $\Gamma = 4.8^{+1.1}_{-0.9}$. Synchronizing to the first X-ray flare, the spectrum slightly became hard, and switched to re-softening during its decaying phase which includes the steepest index of $\Gamma = 5.3^{+0.7}_{-0.6}$. Throughout these fitting, the $N_{\rm H}^{ext}$ parameters keep almost constant. After the first X-ray flare, the photon indices are settled as $\Gamma \sim 2$ which is the typical value for the most X-ray afterglows. The best fit parameters are summarized in table .

4.2. Average Spectrum Obtained by Suzaku/XIS and HXD

In the previous subsection, for the *Suzaku* data, we devided the entire spectra into 5 time intervals as listed in table . We succesfully fitted these spectra with the absorbed simple power-law model, and found no significant spectral evolution. Therefore, we investigated the average spectrum for late X-ray afterglow to determine the spectral parameters.

We performed spectral fitting for the time averaged data combined with both the *Suzaku*/XIS and HXD-PIN. For the HXD-PIN data, For the HXD-PIN fitting, we subtract only the NXB from the observed data, and the CXB is included as the fixed function. A reproduction for the NXB modeling is about 4 % for the nominal HXD observations, so we include this systematics when we subtract the NXB spectrum. Gruber et al. (1999) estimated the functional form of CXB Using their result (see equation 1 in their paper), we simulated an expected CXB spectrum observed by the HXD-PIN. with the flat field RMF. After that, we fitted the simulated spectrum with the RMF for the point source, and estimated the functional form as

Table . Fitting results with the single power-law.

No.	$t-t_0$ [sec]	Δt [sec]	Flux [erg/cm^2/s]	Γ	$N_{\rm H}^{\rm ext}$ [10^{22} cm^{-2}]	χ^2_ν
Prompt Tail (*Swift*/XRT)						
1	75.3	7.5	$(1.99^{+0.24}_{-0.21})\times10^{-8}$	$1.51^{+0.04}_{-0.03}$	$5.10^{+0.99}_{-0.82}$	1.12
2	82.8	7.5	$(9.67^{+1.49}_{-1.23})\times10^{-9}$	$1.59^{+0.11}_{-0.11}$	$3.41^{+0.85}_{-0.71}$	1.12
3	90.3	7.5	$(5.11^{+0.77}_{-0.66})\times10^{-9}$	$1.67^{+0.13}_{-0.12}$	$2.16^{+0.62}_{-0.53}$	0.51
4	97.8	7.5	$(3.68^{+0.75}_{-0.59})\times10^{-9}$	$1.77^{+0.17}_{-0.15}$	$2.45^{+0.93}_{-0.72}$	0.89
5	105.3	7.5	$(2.58^{+0.50}_{-0.42})\times10^{-9}$	$1.95^{+0.18}_{-0.17}$	$2.62^{+0.80}_{-0.66}$	1.15
6	112.8	7.5	$(1.75^{+0.46}_{-0.35})\times10^{-9}$	$2.17^{+0.25}_{-0.23}$	$2.86^{+1.08}_{-0.91}$	0.76
7	124.1	15.0	$(1.02^{+0.19}_{-0.16})\times10^{-9}$	$2.18^{+0.21}_{-0.19}$	$1.94^{+0.63}_{-0.54}$	1.14
8	139.1	15.0	$(4.99^{+1.16}_{-0.92})\times10^{-10}$	$2.52^{+0.28}_{-0.24}$	$2.23^{+0.78}_{-0.65}$	1.21
9	156.6	20.0	$(2.11^{+0.53}_{-0.41})\times10^{-10}$	$2.89^{+0.35}_{-0.30}$	$2.35^{+0.80}_{-0.66}$	1.06
10	176.1	19.0	$(1.30^{+0.49}_{-0.34})\times10^{-10}$	$3.48^{+0.47}_{-0.39}$	$3.35^{+1.36}_{-1.10}$	0.95
11	200.8	30.4	$(6.74^{+1.70}_{-1.33})\times10^{-11}$	$3.47^{+0.43}_{-0.37}$	$2.26^{+0.78}_{-0.65}$	0.72
12	231.3	30.4	$(7.52^{+3.44}_{-2.18})\times10^{-12}$	$4.82^{+1.13}_{-0.88}$	$2.40^{+1.41}_{-1.05}$	0.87
First Flare (*Swift*/XRT)						
13	268.1	43.0	$(5.84^{+1.64}_{-1.17})\times10^{-11}$	$3.43^{+0.39}_{-0.33}$	$2.53^{+0.89}_{-0.68}$	1.25
14	311.1	43.0	$(5.79^{+1.11}_{-0.90})\times10^{-11}$	$3.87^{+0.33}_{-0.29}$	$2.61^{+0.59}_{-0.50}$	1.10
15	354.1	43.0	$(8.71^{+2.32}_{-1.72})\times10^{-12}$	$5.30^{+0.69}_{-0.59}$	$3.15^{+0.87}_{-0.71}$	1.26
16	398.6	46	$(4.38^{+1.61}_{-1.15})\times10^{-12}$	$4.50^{+1.22}_{-0.95}$	$1.52^{+1.13}_{-0.85}$	1.69
17	522.9	202	$(1.22^{+0.41}_{-0.24})\times10^{-11}$	$2.25^{+0.41}_{-0.27}$	$0.19^{+0.74}_{-0.19}$	1.19
Second Flare (*Swift*/XRT)						
18	679.8	111	$(2.25^{+0.72}_{-0.51})\times10^{-11}$	$3.14^{+0.49}_{-0.40}$	$2.13^{+0.97}_{-0.74}$	0.84
19	851.8	234	$(1.88^{+0.48}_{-0.38})\times10^{-11}$	$2.42^{+0.35}_{-0.31}$	$1.08^{+0.69}_{-0.54}$	1.00
20	1085	234	$(1.36^{+1.12}_{-0.57})\times10^{-11}$	$2.25^{+0.73}_{-0.58}$	$2.76^{+3.21}_{-2.21}$	0.40
21	1377	350	$(9.33^{+4.31}_{-2.80})\times10^{-12}$	$2.55^{+0.50}_{-0.40}$	$2.71^{+1.86}_{-1.33}$	1.03
22	1728	352	$(9.00^{+5.06}_{-2.88})\times10^{-12}$	$2.81^{+0.61}_{-0.46}$	$4.08^{+2.19}_{-1.53}$	0.92
Late Afterglow (*Suzaku*/XIS)						
23	39262	2942	$(1.13^{+0.20}_{-0.15})\times10^{-12}$	$2.17^{+0.21}_{-0.19}$	$2.27^{+1.64}_{-1.48}$	1.06
24	45210	2551	$(7.24^{+1.89}_{-1.36})\times10^{-13}$	$1.93^{+0.27}_{-0.15}$	$1.39^{+3.54}_{-0.37}$	0.55
25	58234	16631	$(3.81^{+0.82}_{-0.65})\times10^{-13}$	$2.04^{+0.21}_{-0.18}$	$2.24^{+1.90}_{-1.25}$	0.54
26	74320	13365	$(1.83^{+0.53}_{-0.33})\times10^{-13}$	$2.10^{+0.30}_{-0.24}$	$0.63^{+2.14}_{-0.63}$	1.16
27	90868	14787	$(1.54^{+0.24}_{-0.22})\times10^{-13}$	$2.02^{+0.26}_{-0.20}$	$1.12^{+1.75}_{-1.12}$	0.50

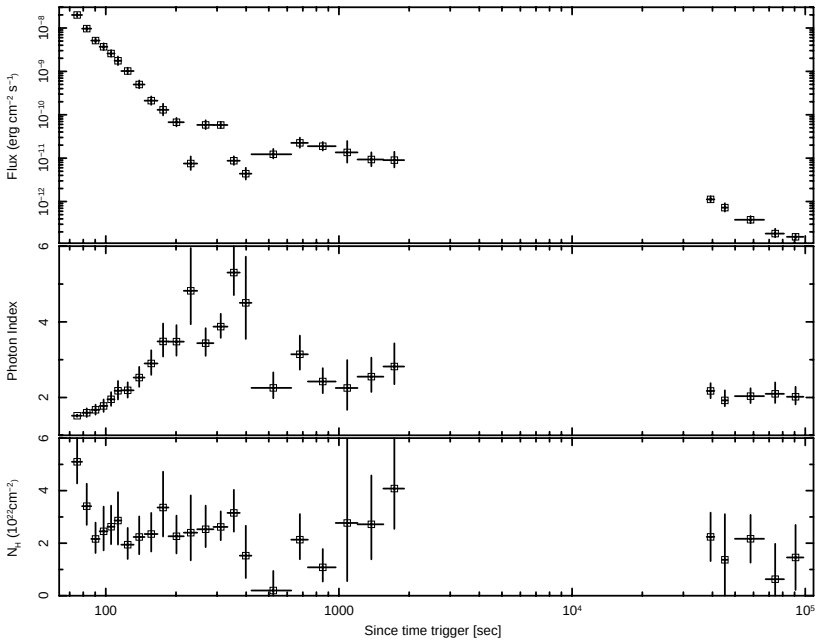

Fig. 2. The temporal histories of 2–10 keV energy flux (top), photon index (middle) and the absorption (bottom) for the X-ray afterglow of GRB 060904A, respectively.

$$\frac{dN}{dE} = 8.134 \times 10^{-4} \Big(\frac{E}{1\ \mathrm{keV}}\Big)^{-1.29} \exp\Big(-\frac{E}{41.13\ \mathrm{keV}}\Big)\ \mathrm{photons\ keV^{-1} cm^{-2} sec^{-1}}. \quad (1)$$

at 10–40 keV range. Detail description is appeared in *** Fujimoto et al. *** in this issue.

In figure 3, we show the averaged spectrum observed with the *Suzaku*/XIS and HXD-PIN. We adopt the absorbed power-law model as described in the previous subsection, and determined the photon index of $\Gamma = 2.00 \pm 0.09$ and the column density of $N_{\mathrm{H}}^{ext} = 5.58^{+3.50}_{-2.19} \times 10^{21}$ cm^{-2}. The observed flux in 2–10 keV band is $F_{2-10} = (3.69 \pm 0.31) \times 10^{-13}$ erg cm^{-2}s^{-1}. Extraporating this photon index toward the HXD-PIN band, we estimated the upper-limit flux in 10–40 keV band. Then we set upper-limit flux in 10–40 keV band of $F_{10-40} < 1.15 \times 10^{-11}$ erg cm^{-2}s^{-1} (90 % confidence).

5. Advanced Spectral Analyses

Let us investigate the detail spectral evolutions. In figure 4, we show the several representative spectra in different time interval on the same figure. We can recognize the strong spectral softening. The flux of harder X-ray band shows the rapid decline while one below 1.0 keV hardly decay at all. This trend was clearly observed in the decaying phase of first X-ray flare. When we assume the standard synchrotron radiation via the accelerated electrons with the power-law energy distribution (γ_e^{-p}), the energy index of photon spectrum can be described as $\nu^{-p/2}$ for the fast cooling regime. In this case, the photon index of $\Gamma = 5.3$ is equivalent to the electron's energy distribution of $\gamma_e^{-8.6}$. This ultra steep index can not lead us to consider the efficient acceleration any more. Although the simple power-law model is

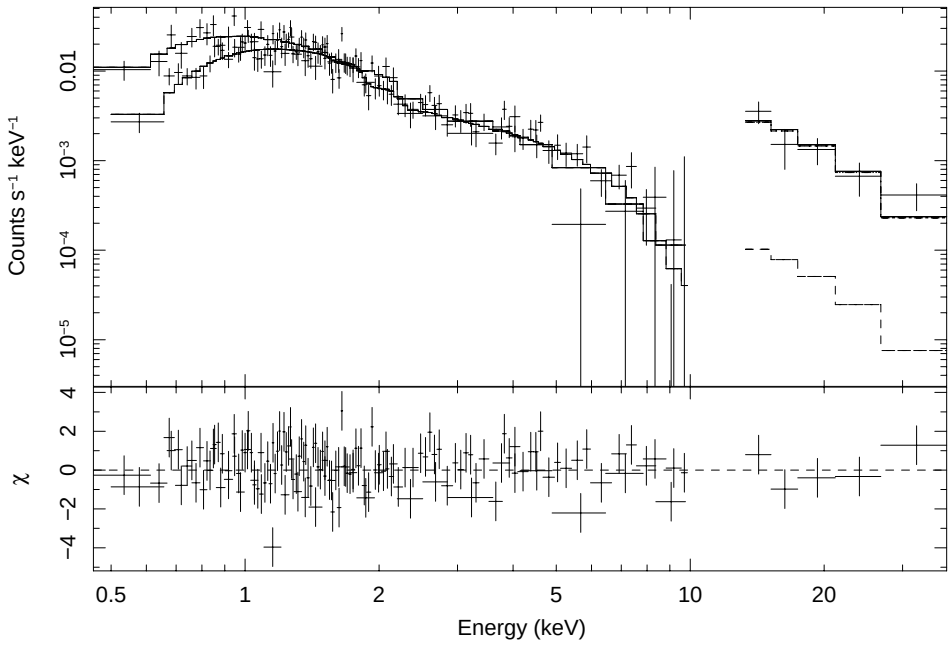

Fig. 3. The spectrum of X-ray afterglow of GRB 060904A observed by the *Suzaku*/XIS and HXD-PIN. The black and red colors indicate a summed spectrum of front-illuminated chips and back-illuminated chip, respectively. The blue spectrum includes the CXB component, and the upper-limit flux is described by the dotted line.

acceptable as shown in table , the ultra soft spectra deviate from the standard synchrotron scinario. Some advanced spectral models may be required. In this section, we give a possible model to explain the observed softening.

5.1. Broken Power-law with Exponential Cutoff (BPEC) Fitting

The spectra of prompt emissions can be well described by the empirical Band function, which is composed by the exponentially connected broken power-law, for typical GRBs. The well determined parameters of the photon indices for the low and high energy band are $\alpha \sim -1.5$ and $\beta \sim -2.25$, respectively. Therefore, it is too hard to explain the very steep photon index found in GRB 060904A spectrum.

Then we performed the advanced spectral analyses based on an assumption which correspond to the broken power-law with exponential cutoff (BPEC) model. Here we used the broken power-law instead of the Band function because the break energy on the Band function can be determined only when $10 \leq E_0 \leq 10^4$ keV in the standard analysis package "XSPEC". In the BPEC model, we denote several parameters as following:

1. $E^{-\Gamma_1}$: $\Gamma_1 \sim 1.5$ between $\nu_c < \nu < \nu_m$ for the fast cooling case. Here ν_c and ν_m are the frequency determined by the cooling time and the minimum electron energy, respectively. Hereafter we denote the break energy as $E_1 \equiv h\nu_m$ which correspond the peak energy in the Band function.
2. $E^{-\Gamma_2}$: $\Gamma_2 \sim 2.25$ between $\nu > \nu_m$ for the power-law index of electron energy distribution

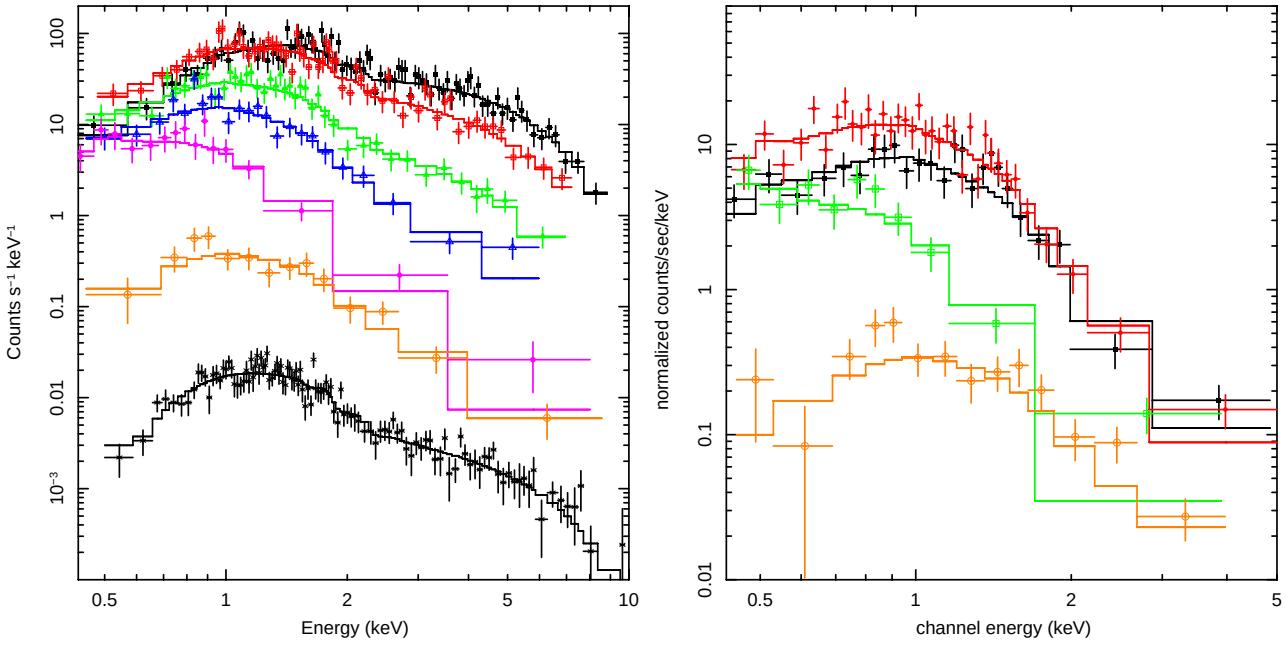

Fig. 4. The spectral evolution of early X-ray afterglow of GRB 060904A with the best fit power-law model listed in table . The left panel shows 6 time-resolved spectra (number 1:black, 3:red, 7:green, 9:blue, 12:magenta, see figure 1) as well as one of the shallow decay part (21:orange). The right panel shows same as the left one for the X-ray flare around ~ 300 sec. Each colour corresponds the spectrum of different time intervals (13:black, 14:red, 16:green).

of $p = 2.5$ (fast cooling case).

3. $\exp(-E/E_2)$: We introduce a cutoff component above the higher energy ends to describe the spectra with very steep photon indices. Several possible physical interpretations will be discussed in the following section.
4. $E^{-\Gamma_3}$: We use an additional power-law component to describe the X-ray afterglow emission at the shallow decay phase.

We performed spectral fitting with the BPEC model for 22 data set observed by the *Swift*/XRT. The best fit results are summarized in table . The blank spaces mean that the BPEC model is out of energy range covered by the *Swift*/XRT. The spectra obtained by the *Suzaku* observation can be fitted by the single power-law with $\Gamma_3 \sim 2$ which are already listed in the table .

We succeeded to fit the XRT spectra with the BPEC model. We found the E_1 (equivalent to the peak energy :E_p) passed through the XRT energy band during the time interval of No. 3–5. After that, the spectra can be described by the single power-law with the photon index of $\Gamma_2 \sim 2.25$. The exponential cutoff energy (E_2)

5.2. Power-law plus Blackbody Fitting

We also investigated a possibility to fit the spectra using the power-law with the blackbody model as suggested by Butler 2006. The high energy end of the blackbody spectrum is

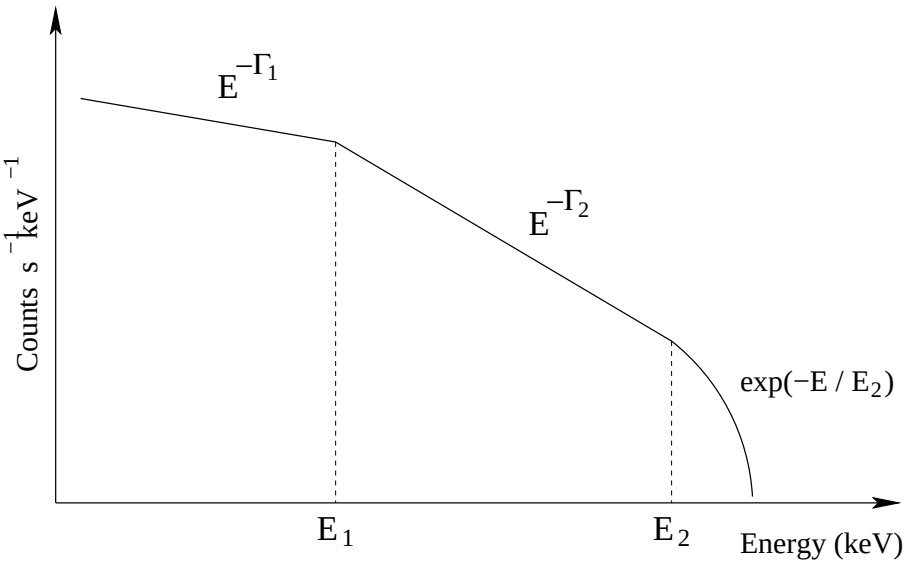

Fig. 5. The model function.

equivalent to the exponential shape. Therefore, this model may enable to represent the BPEC model. To describe the steep spectra by the blackbody component, we fixed the photon indices as $\Gamma = 2.25$ for the spectra steeper than its value. We still keep the the column density as a free parameter.

We summarize the vest fit result in table . We can obtain the acceptable results for almost all cases. As the X-ray intensity of the prompt tail emission grew dimmer, the blackbody temperature roughly bocomes cooler. This property is also observed in GRB 060218 reprted by Butler 2006. However the column density ($N_{\rm H}^{gal}$) also shows significant variation correlated with the blackbody temperature. We could not find this $N_{\rm H}^{gal}$ variation in the spectral fitting both with the single power-law model and the BPEC model, so this fact is caused by the introducing the blackbody component. Therefore the blackbody model may be inappropriate to describe the observed spectral softening.

6. Afterglow Component in the Prompt Tail and the X-ray Flare

In the previous section, we devided the *Swift* and *Suzaku* data with short time intervals to investigate the detail temporal history of spectral evolution. The spectra of prompt tail emission significantly become softer, and we detect the passage of the typical break energy through the *Swift*/XRT window. However, in that analyses, it is difficult to distinguish the X-ray afterglow from the prompt tail and/or the X-ray flare because the photon statistics at the high energy band become poor. Therefore, to improve this fact, we combined several spectra showing the photon indices softer than $\Gamma > 4$ for the purpose of investigating the spectral shape upto 10 keV.

In figure 6, we show the X-ray spectrum at the time interval of 12 + 15 + 16 (black),

No.	Γ_1	E_1 [keV]	Γ_2	E_2 [keV]	Γ_3 afterglow	$N_{\rm H}^{gal}$ [10^{20} cm^{-2}]	$N_{\rm H}^{ext}$ [10^{22} cm^{-2}]	χ^2_ν
1	$1.48^{+0.04}_{-0.05}$	$62.4^{+16.0}_{-17.5}$	2.25(fix)	.....	.....	1.41(fix)	$4.77^{+0.94}_{-0.61}$	0.96
2	$1.54^{+0.06}_{-0.08}$	$41.4^{+19.3}_{-16.0}$	2.25(fix)	.....	.....	1.41(fix)	$3.16^{+0.77}_{-0.64}$	1.16
3	1.50(fix)	$8.62^{+3.27}_{-2.85}$	2.25(fix)	.....	.....	1.41(fix)	$1.61^{+0.37}_{-0.31}$	1.06
4	1.50(fix)	$3.14^{+0.97}_{-0.71}$	2.25(fix)	.....	.....	1.41(fix)	$1.83^{+0.57}_{-0.70}$	0.96
5	1.50(fix)	$2.28^{+0.86}_{-0.42}$	2.25(fix)	.....	.....	1.41(fix)	$1.75^{+0.50}_{-0.42}$	1.18
6	1.50(fix)	< 1.50	$2.18^{+0.23}_{-0.23}$	.....	.....	1.41(fix)	$2.22^{+1.40}_{-0.93}$	0.76
7	1.50(fix)	< 1.42	$2.17^{+0.21}_{-0.19}$	.....	.....	1.41(fix)	$1.37^{+1.01}_{-0.52}$	1.14
8	.....	.....	$2.53^{+0.28}_{-0.25}$	> 5.78	.....	1.41(fix)	$2.24^{+0.78}_{-0.66}$	1.21
9	.....	.....	2.25(fix)	$3.59^{+3.80}_{-1.41}$	.....	1.41(fix)	$1.81^{+0.57}_{-0.47}$	1.16
10	.....	.....	2.25(fix)	$1.69^{+0.82}_{-0.49}$	.....	1.41(fix)	$2.28^{+0.91}_{-0.75}$	0.83
11	.....	.....	2.25(fix)	$1.52^{+0.72}_{-0.46}$	.....	1.41(fix)	$1.53^{+0.55}_{-0.46}$	0.73
12	.....	.....	2.25(fix)	$0.52^{+0.32}_{-0.17}$	.....	1.41(fix)	$1.46^{+0.49}_{-0.77}$	0.97
13	.....	.....	2.25(fix)	$1.51^{+0.64}_{-0.41}$	.....	1.41(fix)	$1.83^{+0.62}_{-0.48}$	1.16
14	.....	.....	2.25(fix)	$1.09^{+0.30}_{-0.23}$	.....	1.41(fix)	$1.70^{+0.41}_{-0.35}$	1.12
15	.....	.....	2.25(fix)	$0.42^{+0.11}_{-0.08}$	.....	1.41(fix)	$2.13^{+0.31}_{-0.28}$	0.84
16	.....	.....	2.25(fix)	$0.16^{+0.06}_{-0.04}$	2.25(fix)	1.41(fix)	$1.26^{+1.25}_{-0.85}$	1.16
17	.....	.....	.....	.....	$2.25^{+0.41}_{-0.23}$	1.41(fix)	< 0.94	1.19
18	.....	.....	2.25(fix)	$2.23^{+2.17}_{-0.89}$		1.41(fix)	$1.53^{+0.65}_{-0.50}$	0.91
19	.....	.....	.....	.....	$2.42^{+0.35}_{-0.31}$	1.41(fix)	$1.08^{+0.69}_{-0.54}$	1.00
20	.....	.....	.....	.....	$2.25^{+0.73}_{-0.58}$	1.41(fix)	$2.76^{+3.21}_{-2.21}$	0.40
21	.....	.....	.....	.....	$2.55^{+0.50}_{-0.40}$	1.41(fix)	$2.71^{+1.86}_{-1.33}$	1.03
22	.....	.....	.....	.....	$2.81^{+0.61}_{-0.46}$	1.41(fix)	$4.08^{+2.19}_{-1.53}$	0.92

Table . Fitting results with broken power-law with exponential cutoff model.

and the average spectrum of late time afterglow observed by *Suzaku* (red). The XRT spectrum shows a clear hardening break around 2 keV. The spectral slope above 2 keV is consistent with the late time X-ray afterglow spectra obtained by *Suzaku*. Therefore, we may enable to recognize this hardening break as the mixing of the X-ray afterglow and the prompt tail (and/or the X-ray flare). We fitted the cut-off power-law component plus the single power-law representing the prompt tail and the behind X-ray afterglow, respectively.

Table . Fitting results by a power-law with blackbody model.

No.	Γ	Flux (PL) [erg cm^{-2}s^{-1}]	kT [keV]	Flux (BB) [erg cm^{-2}s^{-1}]	$N_{\rm H}^{ext}$ [10^{22} cm^{-2}]	χ^2_ν
1	$1.49^{+0.04}_{-0.04}$	$(1.45^{+0.18}_{-0.17})\times10^{-8}$	$3.50^{+0.56}_{-0.52}$	$(4.22^{+1.36}_{-1.37})\times10^{-9}$	$4.01^{+0.88}_{-0.73}$	0.83
2	$1.70^{+0.12}_{-0.09}$	$(9.35^{+1.61}_{-1.21})\times10^{-9}$	$7.34^{+3.65}_{-2.44}$	$(4.41^{+2.83}_{-2.54})\times10^{-10}$	$3.82^{+1.04}_{-0.81}$	1.16
3	$1.84^{+0.13}_{-0.09}$	$(7.29^{+0.97}_{-0.96})\times10^{-9}$	$2.71^{+2.56}_{-2.41}$	$(9.86^{+13.8}_{-9.26})\times10^{-10}$	$2.47^{+0.59}_{-0.51}$	1.04
4	$1.71^{+0.16}_{-0.16}$	$(4.61^{+2.20}_{-1.77})\times10^{-9}$	$0.69^{+0.23}_{-0.15}$	$(1.31^{+0.84}_{-0.90})\times10^{-9}$	$1.61^{+0.99}_{-0.81}$	0.91
5	$1.95^{+0.33}_{-0.22}$	$(4.49^{+1.09}_{-1.55})\times10^{-9}$	$0.84^{+2.63}_{-146}$	$(3.13^{+7.87}_{-3.13})\times10^{-10}$	$2.41^{+0.77}_{-0.62}$	1.45
6	$1.84^{+0.51}_{-0.84}$	$(3.36^{+2.66}_{-2.45})\times10^{-9}$	$0.25^{+200}_{-0.25}$	$(5.98^{+22.0}_{-5.98})\times10^{-10}$	$2.67^{+3.57}_{-1.94}$	0.78
7	$2.95^{+0.91}_{-0.70}$	$(2.12^{+0.90}_{-0.53})\times10^{-9}$	$1.47^{+199}_{-0.39}$	$(6.66^{+28.0}_{-5.06})\times10^{-10}$	$3.07^{+1.58}_{-1.15}$	1.09
8	2.25(fix)	$(1.23^{+0.20}_{-0.22})\times10^{-9}$	$0.18^{+0.09}_{-0.05}$	$(3.21^{+10.6}_{-2.35})\times10^{-10}$	$2.40^{+1.67}_{-0.83}$	1.13
9	2.25(fix)	$(5.89^{+1.38}_{-1.67})\times10^{-10}$	$0.20^{+0.10}_{-0.07}$	$(2.33^{+7.65}_{-1.23})\times10^{-10}$	$1.72^{+1.66}_{-0.79}$	1.09
10	2.25(fix)	$(2.19^{+1.68}_{-1.70})\times10^{-10}$	$0.31^{+0.03}_{-0.07}$	$(3.20^{+0.97}_{-0.87})\times10^{-10}$	$0.41^{+1.09}_{-0.41}$	0.83
11	2.25(fix)	$(1.91^{+0.86}_{-1.00})\times10^{-10}$	$0.23^{+0.06}_{-0.06}$	$(1.78^{+1.05}_{-0.53})\times10^{-10}$	$0.66^{+0.81}_{-0.63}$	0.90
12	2.25(fix)	$(6.69^{+4.14}_{-4.61})\times10^{-11}$	$0.14^{+0.04}_{-0.03}$	$(1.60^{+3.68}_{-0.87})\times10^{-10}$	$1.08^{+1.45}_{-0.98}$	0.61
13	2.25(fix)	$(1.15^{+0.62}_{-0.67})\times10^{-10}$	$0.26^{+0.04}_{-0.04}$	$(1.67^{+0.42}_{-0.38})\times10^{-10}$	$0.68^{+0.56}_{-0.48}$	0.90
14	2.25(fix)	$(1.49^{+0.56}_{-0.58})\times10^{-10}$	$0.22^{+0.03}_{-0.03}$	$(2.83^{+0.77}_{-0.54})\times10^{-10}$	$0.69^{+0.47}_{-0.39}$	1.02
15	2.25(fix)	$(8.99^{+3.80}_{-3.99})\times10^{-11}$	$0.14^{+0.02}_{-0.02}$	$(3.10^{+2.64}_{-1.16})\times10^{-10}$	$1.47^{+0.77}_{-0.60}$	0.88
16	2.25(fix)	$(4.65^{+2.20}_{-2.35})\times10^{-11}$	$0.12^{+0.03}_{-0.03}$	$(7.89^{+22.2}_{-4.64})\times10^{-11}$	$0.86^{+1.18}_{-0.75}$	1.08

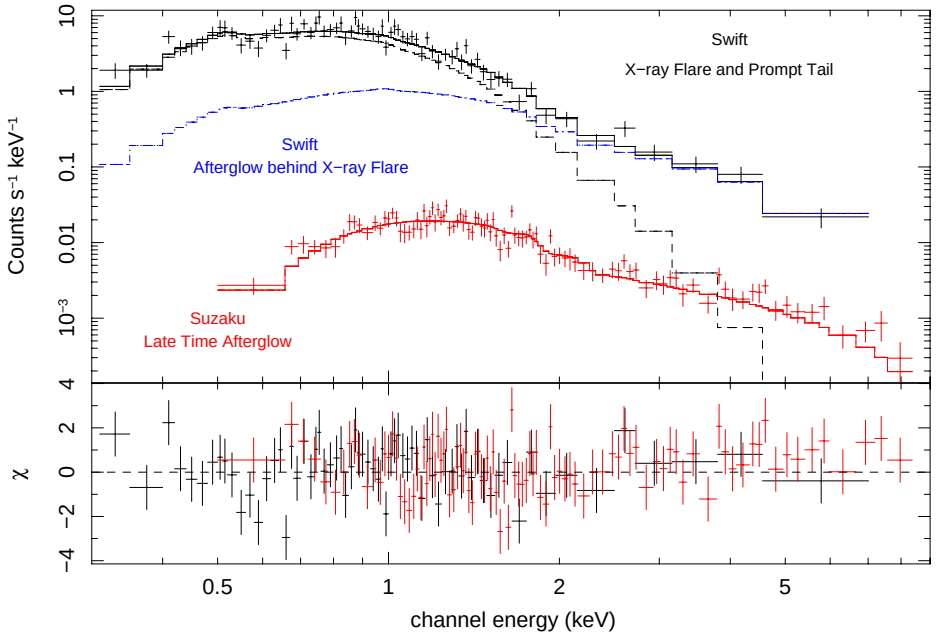

Fig. 6. Time resolved spectrum selected during the time interval with the photon index $\Gamma > 4$ (12, 15 and 16). The spectrum breaks around 2 keV, and the photon index changes harder toward the harder energy band. This spectrum can be fitted with two power-law model

7. Discussions

We found the significant spectral softening during the prompt tail emission and X-ray flate of GRB 060904A. The photon index evolves from $\Gamma = 1.5$ to $\Gamma = 5.3$, which is one of the strongest softening ever observed. Moreover, we found simillar spectral softening in the X-ray flare. We think there are two noticable points to be discussed. One is the time profile of the spectral break energy, especially based on the curvature effect. Another is a possible origin of the ultra steep spectrum and/or the exponentical cutoff.

7.1. Time Profile of Spectral Break Energy

In figure 7, we show the observed time history of the spectral break energy. The open and filled squares indicate the E_1 and E_2 profiles of the prompt tail emission, measured from the most intense peak at $t - t_0 = 55$ sec, respectively. The first point of open square is represented by the peak energy of $E_p = 163 \pm 31$ measured from the average spectrum observed *Konus-Wind* (Golenetskii 2006). The open triangles are one of E_2 in the X-ray flare measured from $t - t_0 = 268.1$ sec. We can recognize that the time profiles of break energies are very similar to each other. When we adopt a power-law model for each time profile, we obtained

$$E_{break} \propto \begin{cases} t^{-3.9\pm0.8} & \text{for } E_1 \text{ of prompt tail} \\ t^{-3.1\pm2.5} & \text{for } E_2 \text{ of prompt tail} \\ t^{-1.7\pm0.6} & \text{for } E_2 \text{ of X-ray flare.} \end{cases} \tag{2}$$

When we assume a instantaneous emission from the relativistic shell, a delayed emission caused by a geometrical curvature of emitting material is expected. This effect is widely called as the curvature effect. The relativistic boosting of delayed emission is much smaller than the on-axis emission. Therefore, the characteristic frequency of prompt emission becomes softer as time goes by.

When we define the point where the radial velocity of expanding spherical shell is parallel to the line of sight to be $\theta = 0$, a Doppler factor toward the observer at a high latitude angle θ is given by

$$\delta = \frac{1}{\Gamma(1 - \beta\cos\theta)}. \tag{3}$$

The difference of photon arrival time caused by the geometrical curvature can be described as

$$t - t_0 = \frac{R_0(1 - \cos\theta)}{c}, \tag{4}$$

where R_0 is the radius of emitting material, t_0 is the photon arrival time emitted at $\theta = 0$, and c is the light velocity. For the extremely relativistic case, we can adopt $\beta \sim 1 - 1/2\gamma^2$ and denote the Doppler factor as a function of t;

$$\delta(t) \sim \frac{2\gamma}{1 + (t - t_0)/\tau}, \quad \tau \equiv \frac{R_0}{2\gamma^2 c}. \tag{5}$$

Then the peak energy and the cutoff energy are expected to have the time dependence of

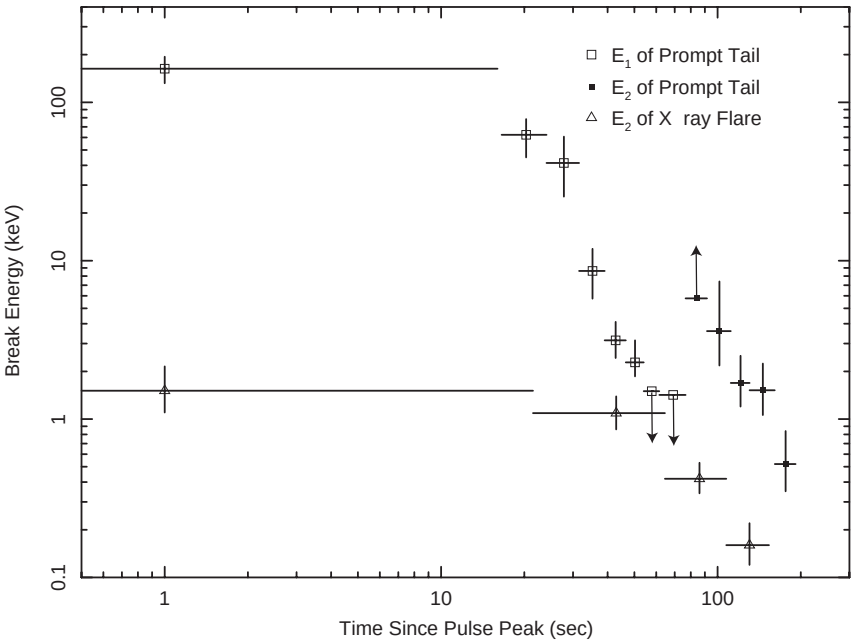

Fig. 7. Time histories of spectral break energy. The open and filled squares mean the break energy E_1 and E_2 of the prompt tail emission measured from the most intense pulse at $t - t_0 = 55$ sec. The open triangles mean the E_2 history of the X-ray flare measured from $t - t_0 = 268.1$. The decay profiles are very similar and the best fit power-law model is $t^{-3\pm1}$.

$$E_{break} = \frac{E_{break,0}}{1 + (t - t_0)/\tau}, \tag{6}$$

if the curvature effect controls the spectral softening. However, we observed the spectral evolution as equation 2, and they are inconsistent with the curvature effect.

Zhang, Liang & Zhang (2006) performed simaltanious studies for 17 early X-ray afterglows observed by *Swift*/XRT, and discussed whether the spectral softening can be explained by the curvature effect or not. According to their results, 7 GRBs show no spectral evolution and the others have significant hard-to-soft trend. They

7.2. Possibility of Ultra Soft Spectra

In the case of GRB 060904A, the blackbody spectrum is not accommodated.

8. Acknowledgment

We thank R. Yamazaki and K. Ioka for the useful discussion about the spectral evolution based on the curvature effect. This research was supported by Grant-in-Aid for Scientific Research of the Japanese Ministry of Education, Culture, Sports, Science and Technology, No.18684007 (DY)

References

Amati, L., et al., 2002, A&A, 390, 81

Butler, N. R., 2006, astro-ph/0604083

Dickey, J. M., & Lockman, F. J., 1999, ARAA, 28, 215

Golenetskii S., Aptekar R., Mazets E., et al., 2006, GCN, 5518

Gruber, D. E., Matteson, J. L., & Peterson, L. E., ApJ, 520, 124, 1999

Nousek, J. A., et al., 2006, ApJ, 642, 389

Pelangeon, A. & Atteia, J.-L. 2006, GCN, 5521

Ryde, F., 2005, ApJ, 625, L95

Ryde, F., et al., 2006, astro-ph/0608363

Sato, G., et al., 2006, astro-ph/0611148

Tashiro, M. S., et al., 2006, astro-ph/0609437

Yonetoku, D., et al., 2004, ApJ, 609, 935

Zhang, B-B., Liang, E-W, & Zhang, B., 2006, astro-ph/0612246